Sādhanā, Vol. 24, Parts 1 & 2, February & April 1999, pp. 5–16. © Printed in India.

Propagation of tides in the Mandovi and Zuari estuaries

SATISH R SHETYE

National Institute of Oceanography, Dona Paula, Goa 403 004, India
e-mail: shetye@csnio.ren.nic.in; shetye@darya.nio.org

Abstract. The Mandovi and the Zuari are two shallow estuaries that are located in Goa and join the Arabian Sea. The main channel of each is about 50 km long, has its cross-sectional area decreasing rapidly in the upstream direction, and receives large amounts of riverine freshwater during the southwest Monsoon and little during the rest of the year. Tides in the channels exhibit the following characteristics: (a) The speed of propagation is about 6.5 m s^{-1}; (b) tidal amplitude remains unchanged over a distance of about 40 km from the mouth; (c) mean water level near the head increases with increase in runoff; (d) tidal amplitude decays rapidly over $\approx$ 10 km near the head, the decay is more rapid during periods of higher runoff.

A nonlinear numerical model based on the equations for conservation of momentum and mass reproduces all the observed features. The model fields show that momentum balance in the channels is primarily between pressure gradient and friction. Assuming such a balance, we formulate a linear analytic model for tidal propagation in a channel whose cross-sectional area decreases exponentially with distance from the mouth and has influx of riverine freshwater at its head. The model solution mimics the observed features (a)–(c) cited above but not (d). Our conjecture is that the quadratic friction term in the momentum balance and the nonlinear term in the continuity equation are essential to simulate the decay of tidal amplitude at the upstream end.

Keywords. Mandovi and Zuari estuaries; tidal propagation; nonlinear numerical model; analytic model.

1. Introduction

An estuary, with sea at one end and river at the other, forms a zone of transition between saline and freshwater. There are probably a couple of hundred estuaries of various sizes distributed along the Indian coastline. Their banks have traditionally been favourite locations for human settlement. As a result, many of India's major cities are located at such places. The estuaries have been used to discharge industrial and domestic waste. With increase in industrial activity and population, many of the estuaries are feared to have reached a state of rapidly deteriorating water-quality due to accumulation of pollutants. In addition, many

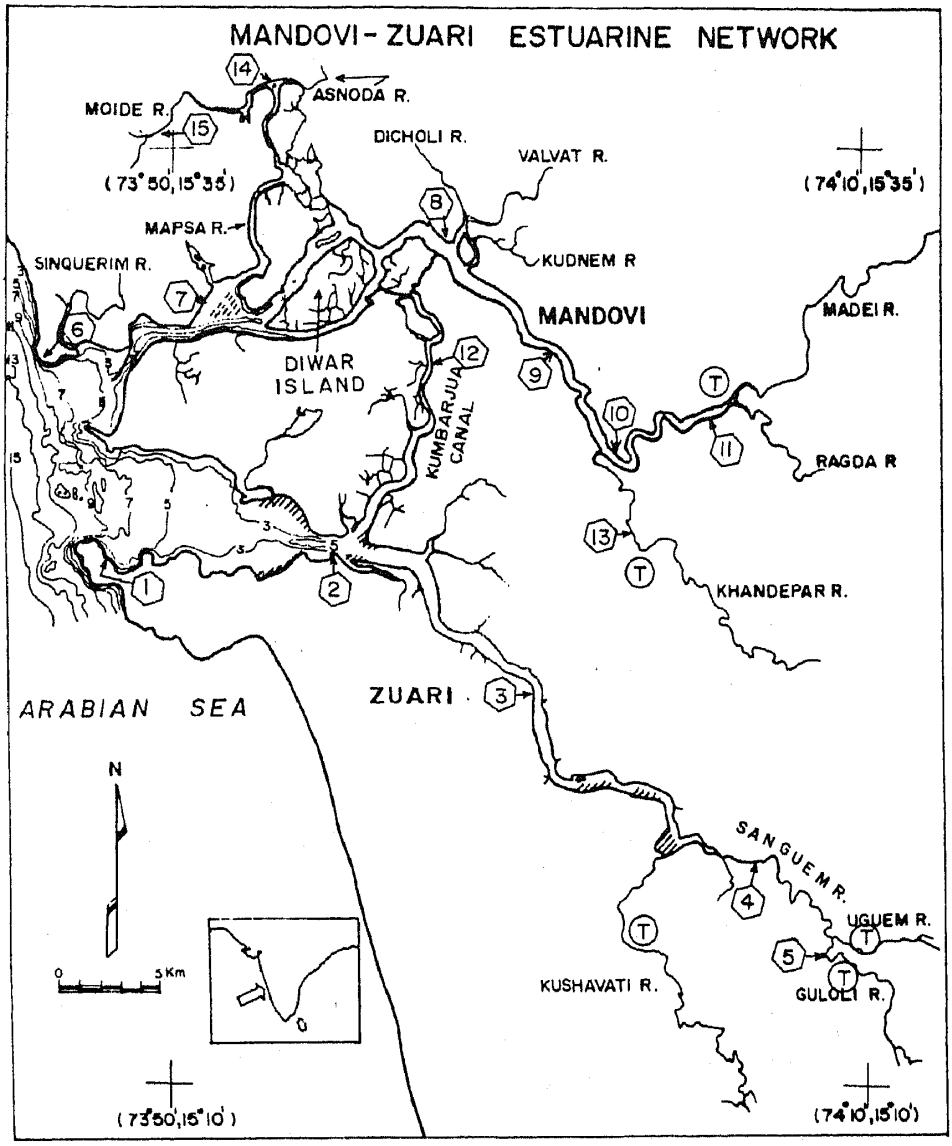

Figure 1. Map of the Mandovi and Zuari estuaries. The depth (m) contours are with respect to mean sea level. To avoid clutter they are shown only near the mouths of the main channels of the Mandovi and the Zuari. "T" in a circle shows location up to which tidal influence is felt. The 15 locations where observations were made during April and August 1993 are shown with a number inside a hexagon – 1: Marmagao; 2: Cortalim; 3: Loutulim; 4: Sanvordem; 5: Sanguem; 6: Aguada; 7: Penha de Franca; 8: Sarmanas; 9: Volvoi; 10: Sonarbaag; 11: Ganjem; 12: Banastarim; 13: Khandepar; 14: Sirsai; 15: Mapsa. Of these, locations 6–11 are referred to in figure 4 below.

of the estuaries have had freshwater brought by the rivers joining them diverted, leading to a change in salinity. Hence it is becoming increasingly apparent that to protect the water-quality and the ecosystems of the Indian estuaries, they will have to be managed. This would be possible only if we understand their physics, chemistry, and biology. One of the more fundamental of these problems is understanding the dynamics of circulation in the estuaries.

A large number of estuarine channels distributed along the coast of India are shallow, about 5 m deep, with width decreasing rapidly with distance from the mouth. The

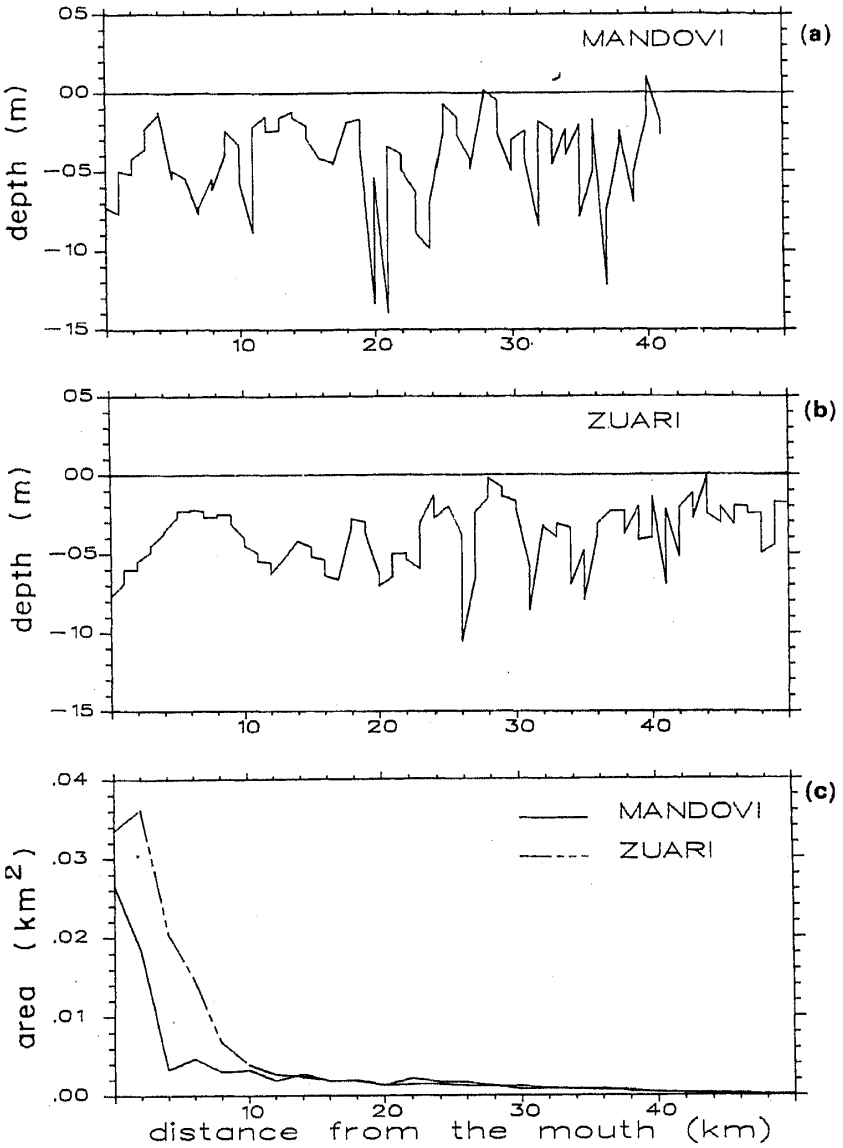

Figure 2. Depth (m) with respect to mean sea level along a line midway through the main channels of (**a**) Mandovi, and (**b**) Zuari. The horizontal scale gives distance (km) from mouth of the two estuaries. (**c**) Cross-sectional area (km) with respect to mean sea level of the main channels of the Mandovi and Zuari. The horizontal axis gives the distance (km) from the mouth of the estuary.

circulation in the channels is forced by oscillatory tidal flow at the mouth, and by river discharge at the head. What is the nature of circulation in such a system? How does the water level and velocity in the channels vary as a function of location and time? To answer questions such as these, a study involving observations and numerical modelling was carried out in the Mandovi and the Zuari estuaries in Goa. Both join the Arabian Sea and their channels are similar to many of those found along the western coast of India. The observations were conducted during April 1993 (dry season) and August 1993 (wet season), and have been reported earlier by Shetye *et al* (1995). The results of the numerical model studies have been discussed by Unnikrishnan *et al* (1997). In the present paper we summarize their findings, and interpret them using a simple analytic model.

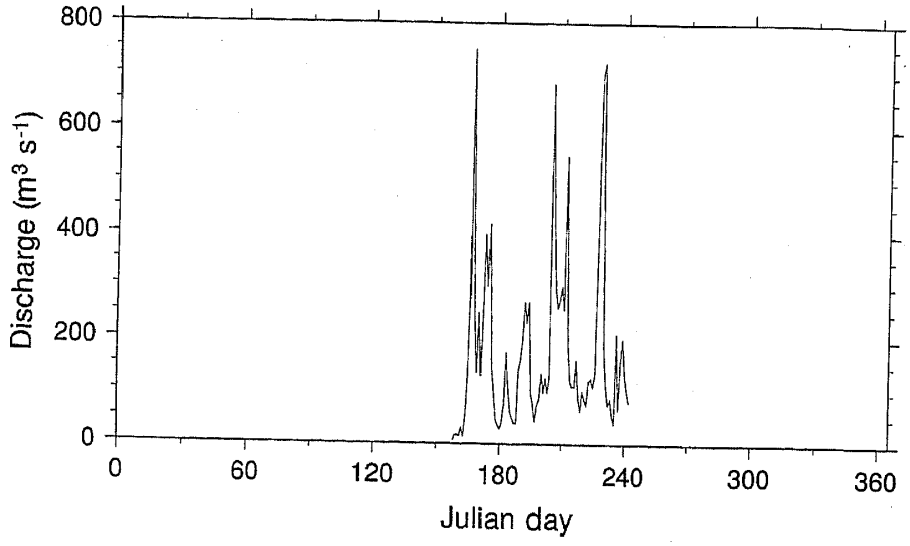

Figure 3. Discharge hodographs of Mandovi River near Ganjem (see figure 1 for location). The horizontal axis gives day of the year 1978 from January 1. The vertical axis gives discharge in cubic metres per second.

The Mandovi and the Zuari are each about 50 km long (figure 1). Though they are used for transport of goods (mainly iron ore), for fishing, and for dumping domestic and industrial waste, the pollution level in the channels is fortunately low. The depth of each of the channels is approximately 5 m on an average, and decreases slowly in the upstream direction, as seen in figures 2a and b. The width of each of the main channels decreases rapidly with distance from the mouth. As a result, the cross-sectional area also decreases rapidly (figure 2c).

Though each of the two main channels receives freshwater through small streams at many points along its length, the river at the upstream end forms the major source of freshwater. Its influx is high during the southwest monsoon (June–October), when most of the precipitation occurs over the catchment area of the rivers that feed the two channels (figure 3). The runoff decreases rapidly after withdrawal of the monsoon. However, even during April–May, the driest part of the dry season, the water remains fresh at the upstream end of each of the channels where, the cross-sectional area being small, even small amounts of runoff is enough to keep the salinity at negligible levels.

The next two sections summarize the main findings of the observations, and of the numerical model study. In § 4 we examine these findings from the point of view of a linear analytic model. Capabilities and limitations of the model are discussed in § 5. Our principal conclusion is that the linear model is successful in explaining the observations along most of the length of the channel, except at its upstream end, where nonlinear effects seem to dominate.

2. Observations

The primary goal of the programme of observations was to record how the water levels in the Mandovi and the Zuari vary with location and time under the influence of tides during two contrasting periods of river runoff – when it is minimal (dry season), and when it is

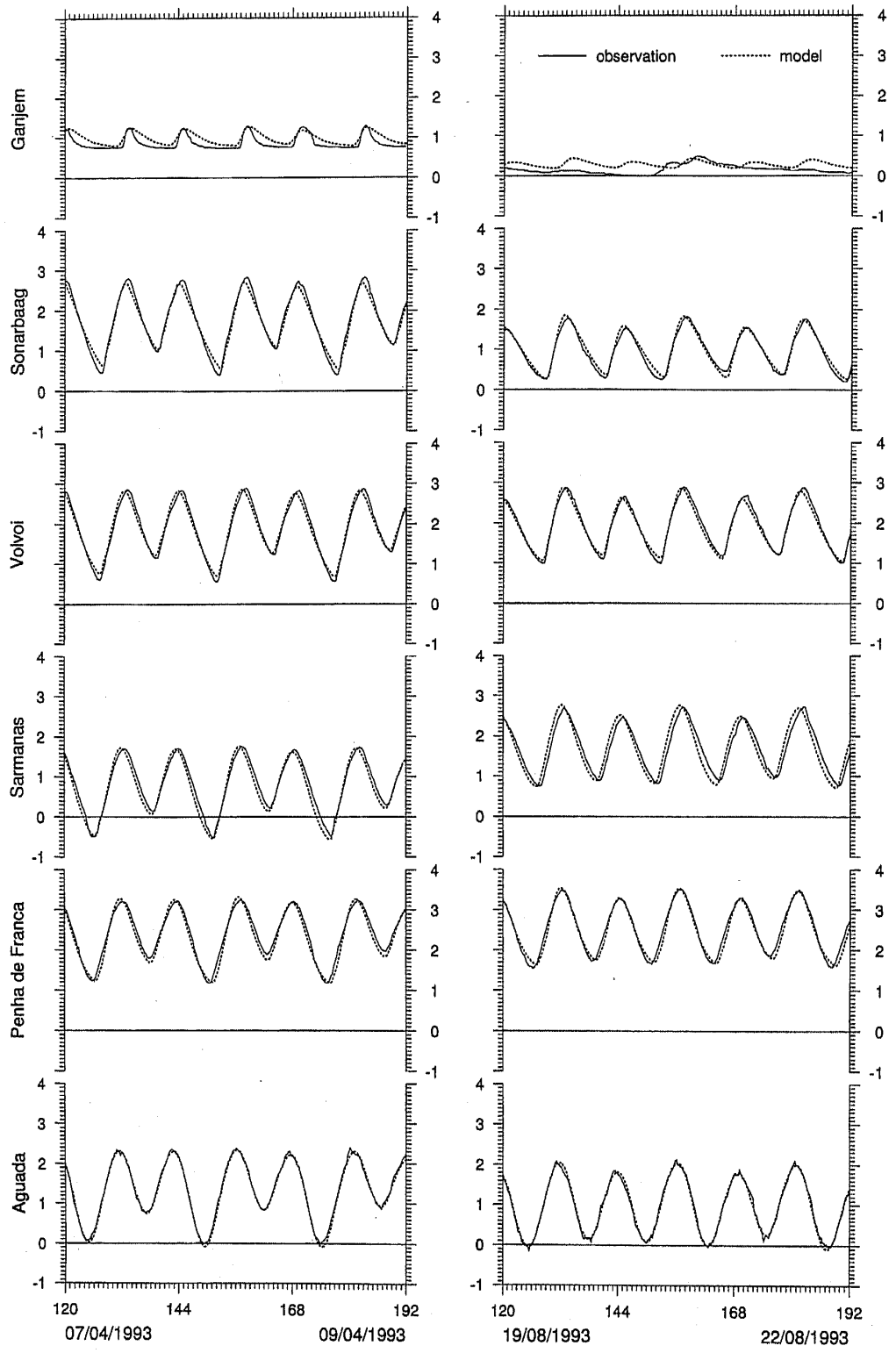

Figure 4. Sea level variation (m) during 7–9 April 1993 (panels on the left), and 19–21 August 1993 (panels on the right) in the Mandovi estuary at Aguada, Penha de Franca, Sarmanas, Volvoi, Sonarbaag, and Ganjem (see figure 1 for locations). The zero on the vertical axis is chosen arbitrarily. The horizontal axis shows the date and hour. In the left hand (right hand) panels 0 hour corresponds to 0000 hours on 2 April (14 August) 1993.

maximal (wet season). The 15 locations where the observations were made are shown in figure 1. At each location the water level was recorded using a tide-pole once every 15 mins for 72 h during each of the two phases of observations. A sample of water was collected every hour for determining salinity. The dry (wet) season observations were carried out during 7–9 April (19–22 August) 1993.

Modification of the tide as it propagates in the main channel of Mandovi is seen in figure 4. At the mouth, Aguada, the tide consists of semi-diurnal and diurnal oscillations, the former being dominant. At the next four upstream locations – Penha de Franca (9.1 km from the mouth), Sarmanas (24.4 km), Volvoi (32.9 km), and Sonarbaag (40.1 km) – the amplitude of the tide remained virtually unchanged. However, at the next station farther upstream, Ganjem (48.1 km from Aguada), the amplitude drops dramatically. During the wet season the water level at Ganjem changes primarily due to variation in runoff.

Figure 5a shows variation of the semi-diurnal amplitude with distance from the mouth of the main channel of the Mandovi during both the wet and the dry seasons. It is seen that for about 40 km from the mouth the amplitude remains unchanged, and then drops sharply over the last 10 km at the upstream end. The variation is similar in both seasons, except that the drop near the upstream end is sharper during the wet season.

The speed of tidal propagation in the channel can be estimated from figure 5b that shows the spatial variation of the phase of the semi-diurnal component. The speed is approximately 6.7 m s^{-1} in both seasons.

During the observations a bench-mark was established near each tide-pole. This permitted determination of the change in mean sea level from the dry to the wet season observations. It is found that the mean water level at the upstream end of the Mandovi (Zuari) is 1.6 m (1 m) higher during the wet season.

3. Numerical model

The purpose of the numerical model study was to identify the dynamics underlying the features seen in the observations. The numerical model used in the study is based on the equations for conservation of momentum and is mass-averaged across the cross-section of an estuarine channel. These are,

$$\frac{\partial Q}{\partial t} + \frac{2Q}{A}q - \frac{2bQ}{A}\frac{\partial h}{\partial t} = -gA\frac{\partial}{\partial x}(z_o + d + h) - g\rho\frac{Q \mid Q \mid}{AC^2R_H}, \tag{1}$$

$$b\frac{\partial h}{\partial t} + \frac{\partial Q}{\partial x} - q = 0, \tag{2}$$

where Q is along-channel transport and h is elevation with respect to mean water level; t and x are respectively time and along-channel coordinate, the latter increases in the upstream direction. The channel is assumed to be rectangular with depth d; z_o is the distance between the bottom of the channel and an arbitrary level surface well below the bottom. Width of the channel is defined by two parameters b_s and b. The former, which is either equal to or smaller than the latter, is the width in which the along-channel flow occurs. The difference between b and b_s determines width of the channel covered with mudflats that act as storage, and do not allow along-channel motion. The cross-sectional area, A, in (1) is given by $b_s(d + h)$. Freshwater influx per unit length of the channel

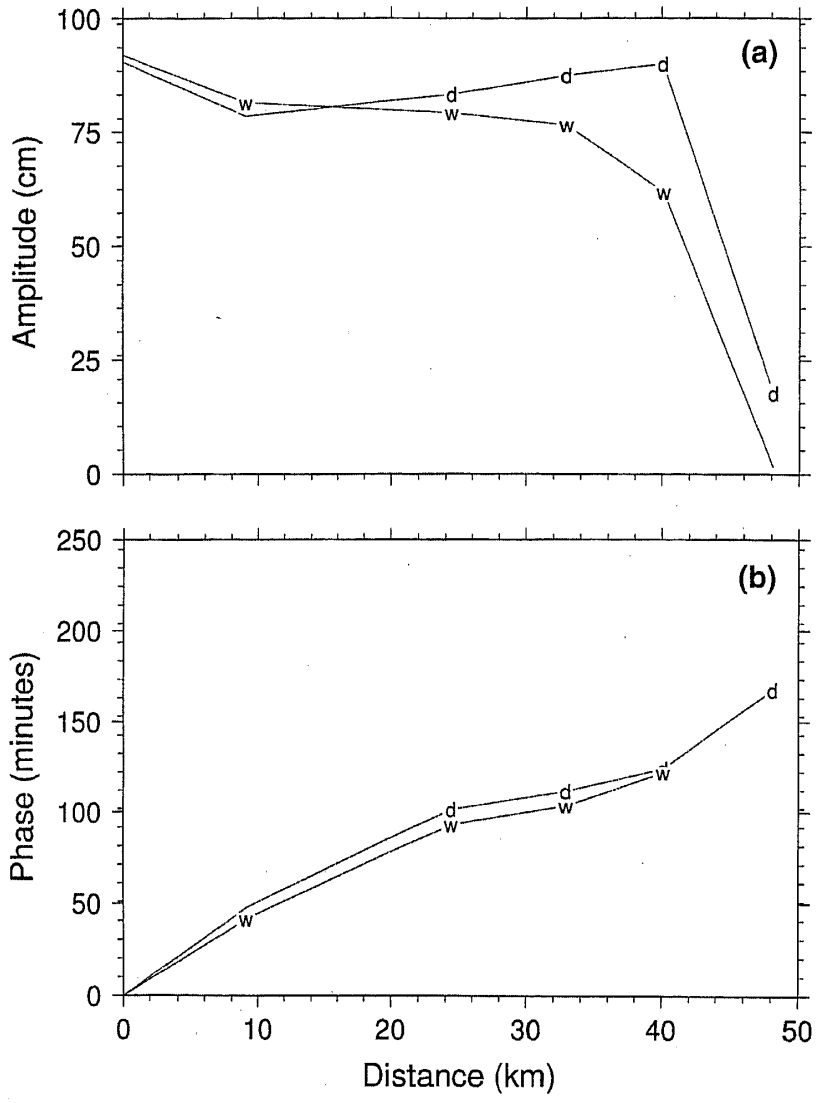

Figure 5. (**a**) Variation of amplitude (cm) of the semi-diurnal component of the tide with distance (km) along the main channel of the Mandovi during the dry season observations, 7–9 April 1993 (marked "d") and wet season observations, 19–21 August 1993 (marked "w"). (**b**) Change of phase (minutes) of the semi-diurnal band in the main channel of the Mandovi with respect to the tide at Marmagao. Variation during the dry season (wet season) observations is marked "d" ("w"). The horizontal axis gives the distance (km) from the mouth of the channel. The phase at the station at the upstream end during the wet season has not been shown because the flow was controlled by freshwater influx and there was no tidal influence.

is given by q, g is the acceleration due to gravity, ρ is the density. The last term on the right hand side of (1) represents frictional dissipation. In this term R_H is the hydraulic radius of the channel defined as (A/P_r) where P_r is the wetted perimeter, C is given by $(1.49/n)R^{1/6}$, where n is the Manning coefficient.

The model is forced at the mouth of each channel by prescribing tidal elevation. Runoff is prescribed at the head. The model simulates the observed water level very well, as seen in figure 4. In particular, the observed features of variation in amplitude, phase, and mean water level are reproduced.

Numerical experiments, in which freshwater influx at the upstream end is changed from experiment to experiment, show that the decay in tidal amplitude at the upstream end of the

channels is proportional to riverine freshwater influx. There is no decay if the freshwater influx is absent.

Analysis of the model fields shows that the momentum balance in each channel is primarily between pressure gradient and friction, the contribution of the local advection term and the nonlinear advection term being small, particularly in the region away from the mouth. This is a useful result because it helps to simplify the dynamics. It is also consistent with observations in shallow estuaries (Brown & Trask 1980) and with earlier theoretical analysis (Le Blond 1978; Friedrichs & Aubrey 1994). In the next section we use such a momentum balance in a linear analytic model.

4. Analytic model

Consider an estuarine channel with its mouth at $x = 0$, and head at $x = L$. Let $b_s = b$, both being dependent on x. This implies that there are no mudflats. We start with (1) and (2) and introduce approximations (a)–(d).

(a) Assume that in (1) the three terms on the left hand side are negligible, i.e. the momentum balance is between pressure gradient and friction.

(b) $(z_o + d)$ is a constant, and $h = h_o + \eta(x, t)$ where h_o is the depth when there is no flow. We further assume that h_o is independent of x. With these approximations the equations for continuity and momentum are respectively,

$$b\frac{\partial \eta}{\partial t} = -\frac{\partial}{\partial x}[b(h_o + \eta)u], \tag{3}$$

and

$$g\frac{\partial \eta}{\partial x} + \rho g\frac{u \mid u \mid}{C^2 R_H} = 0, \tag{4}$$

where u is the velocity and $Q = Au$. We now linearize (3) and (4) by introducing approximations (c) and (d).

(c) In (3) replace $(h_o + \eta)$ by h_o. This implies that $(\eta/h_o) \ll 1$.

(d) In (4) replace the quadratic friction term with linear friction:

$$\rho g\frac{u \mid u \mid}{C^2 R_H} = ru, \tag{5}$$

where r is a constant, as in Friedrichs & Aubrey (1994).

We now let

$$b = b_o \exp[-(x/L_b)], \tag{6}$$

where b_o is width of the channel at the mouth, L_b is the e-folding distance of decrease in channel width. Substituting (5) and (6) in (3) and (4) we get

$$\frac{\partial \eta}{\partial t} = -h_o\frac{\partial u}{\partial x} + \frac{h_o}{L_b}u, \tag{7}$$

and

$$g\frac{\partial \eta}{\partial x} = -ru, \tag{8}$$

which can be combined to write an equation for η,

$$\frac{\partial \eta}{\partial t} - \left(\frac{c_\circ^2}{r}\right)\frac{\partial^2 \eta}{\partial x^2} + \left(\frac{c_\circ^2}{rL_b}\right)\frac{\partial \eta}{\partial x} = 0, \tag{9}$$

where $c_\circ = (gh_\circ)^{1/2}$ is phase velocity of the classical shallow-water surface gravity wave. To determine η when there is tide at the mouth and freshwater influx at the head, we solve (9) with the following boundary conditions.

(1) At $x = 0$, $\eta = \eta_\circ e^{i\omega t}$, where $\eta_\circ$ is the amplitude of the tide at the mouth of the estuary and ω is its frequency.

(2) At $x = L$, $u = -u_f$, where u_f is the speed of riverine freshwater flowing into the channel.

It is instructive to solve (9) as a sum of two cases: (1) tidal flow, that is forced with the tide at the mouth, but has no freshwater influx at the upstream end; and (2) freshwater flow, which has no tide at the mouth, but has freshwater influx at the head. The complete solution is a linear combination of these two problems that are discussed next.

4.1 *Tidal flow*

In this case we solve (9) with the following boundary conditions. At $x = 0$, $\eta = \eta_\circ e^{i\omega t}$, and at $x = L$, $u = 0$. From (8) we note that the boundary condition at $x = L$ can be written as $\partial\eta/\partial x = 0$. Keeping in view the boundary condition at $x = 0$, we look for solutions $\eta \sim e^{i(kx-\omega t)}$, where k is a complex wave number. Substituting this form in (9) we get two possible wave numbers,

$$k_{1,2} = \left(\frac{1}{2L_b}\right)\left[-i \pm i\left(1 - i\frac{4L_b^2\omega r}{c_\circ^2}\right)^{1/2}\right], \tag{10}$$

where k_1 (k_2) corresponds to the choice of +ve (−ve) sign on the right hand side. Using the solutions corresponding to the two wave numbers, and imposing the boundary conditions at $x = 0$ and L, we get

$$\eta(x,t) = -\eta_\circ \frac{k_2 \exp[ik_2 L]}{k_1 \exp[ik_1 L] - k_2 \exp[ik_2 L]} \exp[i(k_1 x - \omega t)] + \eta_\circ \frac{k_1 \exp[ik_1 L]}{k_1 \exp[ik_1 L] - k_2 \exp[ik_2 L]} \exp[i(k_2 x - \omega t)]. \tag{11}$$

The main channels of the Mandovi and the Zuari are each approximately 50 km long, making this a suitable choice for L. We estimate that L_b, the e-folding length of the decrease in the width of the channels of the two estuaries, is about 7.5 km (see figure 2). Following

Friedrichs & Aubrey (1994) we set $r = 1.0 \times 10^{-3}\ \mathrm{s}^{-1}$. We choose $h_\circ$ to be 5 m, which is the average depth of the two estuaries (figure 2). For semi-diurnal tide $\omega = 1.4 \times 10^{-4}\ \mathrm{s}^{-1}$. The choice of $h_\circ$ makes $c_\circ = 7.1\ \mathrm{m\,s}^{-1}$. We then have $\delta = (4L_b^2\omega r/c_\circ^2) \sim 0.1$, allowing us to approximate $k_{1,2}$ in (10) by

$$k_{1,2} \approx \left(\frac{1}{2L_b}\right)\left[-i \pm i\left(1 - i\frac{2L_b^2\omega r}{c_\circ^2}\right)\right], \tag{12}$$

accurate to $\vartheta(\delta)$. To the same accuracy, k_1 and k_2 can be written as

$$k_1 \approx L_b\omega r/c_\circ^2, \tag{13}$$

$$k_2 \approx -(i/L_b) - (L_b\omega r/c_\circ^2). \tag{14}$$

These simpler relations allow us to interpret physically the waves corresponding to the two wave numbers. Wave number k_1, being real, represents a wave that propagates in the direction of positive x without damping, and has wavelength $\lambda = (2\pi c_\circ^2/L_b\omega r)$. For the parameters defined earlier, λ is approximately 300 km, which is about six times larger than L. Hence at any given time only a part of the wave will be seen in the estuarine channel. Another way of looking at this is that the phase difference between the two ends of the estuary will be about $\pi/3$. The phase velocity of the wave, k_1/ω, is $(c_\circ^2/L_b r)$. It represents a surface gravity wave which on entering the estuary has been modified by two effects: friction, which tends to damp it, and geometric confinement, which tends to amplify it during propagation from mouth to head. The wave remains undamped because the two effects cancel each other. Using the values of $c_\circ$, L_b, and r, we get the phase velocity as $6.6\ \mathrm{m\,s}^{-1}$.

The second wave, represented by wave number k_2, propagates in the direction of negative x, and is damped with e-folding distance L_b. Its wavelength and phase velocity are the same as that of the first wave. This wave is generated by reflection of the undamped wave propagating in the positive x direction, and decays because both friction and geometry damp it. Because this wave decays rapidly, it has little impact on tidal propagation, as can be seen from the following relation which has been written by using (13) and (14) in (11), and keeping terms only up to $\vartheta(\delta)$:

$$\eta(x,t) \approx \eta_\circ \exp\left[i\left(\frac{L_b\omega r}{c_\circ^2}x - \omega t\right)\right] - \eta_\circ\left(\frac{L_b^2\omega r}{c_\circ^2}\right) \times \exp\left[-\frac{1}{L_b}(L-x)\right]\exp\left[i\left(\frac{L_b\omega r}{c_\circ^2}(L-x) - \omega t + \frac{\pi}{2}\right)\right]. \tag{15}$$

As seen from this equation, amplitude of the reflected wave decays exponentially away from the upstream end of the estuary. Even at the upstream end, its amplitude is only $\vartheta(\delta\eta_\circ)$, which is much less than $\eta_\circ$, the amplitude of the undamped wave. The tidal propagation in the estuary can therefore be looked upon as consisting of only one wave, the undamped wave, represented by the first term in the above equation. In fact, Friedrichs & Aubrey (1994), in an analytic model similar to ours, did not permit the reflected wave to exist. They achieved this by ignoring the first term on the right hand side of (7). This made their governing equation for η a first-order differential equation which can satisfy only

one boundary condition, and allows only one wave to exist. Ignoring the term essentially means that the rate of change of transport in the estuary arises primarily from change in cross-sectional width, not from change of velocity with distance. This may be fine for the tidal flow, which as we saw earlier has a wavelength that is long in comparison to the length of the estuary. It is, however, not suitable for the case of freshwater flow that is examined next.

4.2 *Freshwater flow*

In this case we assume that the river discharge at the upstream end of the channel is independent of time. Basically, this means that the time-scale associated with temporal variability of the discharge is much longer than the tidal period. The governing equation then is the time-independent version of (9). The boundary condition at $x = L$ is $u = -(g/r)(\partial\eta/\partial x)_{x=L} = -u_f$. The second boundary condition is $\eta = 0$ at $x = 0$. The solution can then be written as

$$\eta = \left(\frac{rL_b u_f}{g}\right) \exp\left[-\frac{(L-x)}{L_b}\right] - \left(\frac{rL_b u_f}{g}\right) \exp\left[-\frac{L}{L_b}\right]. \tag{16}$$

It is easy to see that the second term in the above equation is negligible. The solution implies that in a channel whose cross-sectional area varies exponentially, the mean water level and velocity vary exponentially. Velocity is largest at the upstream end where cross-sectional area is the least. Downstream of this point, as cross-sectional area increases, velocity decreases to conserve transport. Equation (8) links velocity to the gradient of water level, which must then also decrease. When there is no discharge, there is no increase in mean sea-level at the upstream end.

As noted earlier, the observations showed that there is an increase of 1 m in the Zuari and 1.6 m in the Mandovi in the mean sea-level at the upstream end during the wet season. The increase in mean sea-level predicted by (16) is consistent with the observed increase if we choose u_f to be 2 m s^{-1}, which is a reasonable estimate for velocity of river discharge at the upstream end.

5. Discussion

We can now write the essence of the analytic solution for tidal flow in presence of freshwater influx by combining (15) and (16), and by keeping only the most significant term in each equation.

$$\eta(x,t) \approx \eta_o \exp\left[i\left(\frac{L_b \omega r}{c_o^2}x - \omega t\right)\right] + \left(\frac{rL_b u_f}{g}\right) \exp\left[-\frac{(L-x)}{L_b}\right]. \tag{17}$$

The observations summarized in § 2 revealed the following four features of tidal propagation in the Mandovi and Zuari estuaries:

(a) The speed of propagation is approximately 6.5 m s^{-1}.

(b) As the tide propagates from mouth to head, the amplitude of the tide remains unchanged over a large fraction of the length of the main estuarine channels.

(c) The mean sea-level increases at the upstream end during the wet season when freshwater influx increases.

(d) The tidal amplitude decays rapidly in the 10 km stretch at the upstream end of the channel.

Of the four, the first three are reproduced in the analytic solution given above. However, it does not simulate the fourth feature. Hence the analytic model cannot explain the rapid damping of amplitude that is observed at the upstream end of both the Mandovi and the Zuari. The numerical experiments (§ 3) link this damping to freshwater influx. Though the linear model does take freshwater influx into account, it cannot simulate the damping.

Our conjecture is that the damping of the tide near the head is linked to nonlinear interaction between the tidal and freshwater flows. This is ignored in the analytic model. The approximations that delete the nonlinear terms in the governing equations are as below.

(1) Neglect of advection terms (second and third terms on the left hand side of (1)).

(2) Replacing of $(h_o + \eta)$ by h_o in the continuity equation.

(3) Replacing of quadratic friction with linear friction in the momentum equation.

As pointed out in § 3, numerical experiments have shown that the advection term is not significant in the momentum balance. Hence approximation (1) above should be appropriate. Therefore we expect that it is the total height of the water column, $(h_o + \eta)$, and quadratic friction that must be preserved in their nonlinear form to simulate the damping at the upstream end.

References

Brown W S, Trask R P 1980 A study of tidal energy dissipation and bottom stress in an estuary. *J. Phys. Oceanogr.* 10: 1742–1754

Friedrichs C T, Aubrey D G 1994 Tidal propagation in strongly convergent channels. *J. Geophys. Res.* 99: 3321–3336

Le Blond P H 1978 On tidal propagation in shallow rivers. *J. Geophys. Res.* 83: 4717–4721

Shetye S R, Gouveia A D, Singbal S Y, Naik C G, Sundar D, Michael G S, Nampoothiri G 1995 Propagation of tides in the Mandovi–Zuari estuarine network. *Proc. Indian Acad. Sci. (Earth Planet. Sci.)* 104: 667–682

Unnikrishnan A S, Shetye S R, Gouveia A D 1997 Tidal propagation in the Mandovi–Zuari estuarine network, West Coast of India: Impact of freshwater influx. *Estuarine, Coastal Shelf Sci.* 45: 737–744